Scilight

Translational Insights

https://www.sciltp.com/journals/ti



Article

Check for updates

HEK293T Vesicle Lipidomes Retain Core Features of Their Parent Cells

Kyle Peres, Krishna Kishor and Sanjoy K. Bhattacharya *

Miami Integrative Metabolomics Research Center, Bascom Palmer Eye Institute, University of Miami, Miami, FL 33136, USA
* Correspondence: sbhattacharya@med.miami.edu

How To Cite: Peres, K.; Kishor, K.; Bhattacharya, S.K. HEK293T Vesicle Lipidomes Retain Core Features of Their Parent Cells. *Translational Insights* **2026**, *1*(1), 23. https://doi.org/10.53941/ti.2026.100023

Received: 21 July 2026
Revised: 24 August 2026
Accepted: 3 September 2026
Published: 12 October 2026

Abstract: Aims: The extracellular vesicle (EV) membrane is derived from its parent cell. How intact that inheritance is, and whether an EV lipidome is significantly different from unrelated cells and the lipid milieu of circulating plasma has not been subjected to quantitative investigation. We addressed three main questions: (1) whether HEK293T derived EVs share their lipid composition with their parental cell; (2) how varied is the HEK293T EV lipidome when compared to the healthy human plasma lipidome; and (3) whether EV lipidomes from different organs and cell lines (B16, E0771, MC38, etc.) differ from each other. Methods: We analyzed mass spectrometry based lipidomic data generated in house and curated from public repositories, including Metabolomics Workbench. Results: We found that the HEK293T EV lipidome was distinct from unrelated whole cell lipidomes and plasma, while remaining most similar to its parental cell. In HEK293T EVs, most of the detected EV lipids overlapped with HEK293T whole cell lipidome, with moderately conserved abundance patterns. EVs showed selective remodeling with enrichment in sphingomyelin, phosphatidylserine, and diacylglycerol with depletion of triglycerides, lysophosphatidylcholine and phosphatidylinositol. The comparison of EVs across nine different cell lines showed that the tissue of origin was the strongest driver of lipidomic variation in this panel. Conclusions: Within the HEK293T cell line, the EV lipidome reflects its parent cell but is further refined by selective lipid remodeling during EV generation. Because the direct parent cell comparison was limited to HEK293T, this relationship will require validation in additional matched cell and EV systems.

Keywords: lipidomics; exosomes; extracellular vesicles; membrane lipids; comparative lipidomics; mass spectrometry

1. Introduction

Almost every cell in the human body releases extracellular vesicles (EVs). These include many distinct vesicle subtypes, for example exosomes produced through the multivesicular body pathway and microvesicles released from the plasma membrane [1]. Once viewed primarily as a route for cells to discard waste, EVs are now recognized as important mediators of intercellular communication. Through carrying proteins, lipids and nucleic acids between cells EVs provide a mechanism for exchanging molecular information across tissue [1–5]. The lipid bilayer of extracellular vesicles is usually overlooked as a passive container, but it plays an active role in EV function. The vesicle membrane influences uptake, fusion with target cells, and cargo delivery, guiding the biodistribution and signaling of each distinct vesicle.

The consistent theme across EV literature is that the vesicle lipidome is not simply an exact copy of the parent cell membrane. Instead, it is assembled through an active, biochemically regulated sorting process. For example, prior studies have shown that sphingomyelin and cholesterol, two lipids enriched in lipid raft microdomains, are

Copyright: © 2026 by the authors. This is an open access article under the terms and conditions of the Creative Commons Attribution (CC BY) license (https://creativecommons.org/licenses/by/4.0/).
Publisher's Note: Scilight stays neutral with regard to jurisdictional claims in published maps and institutional affiliations.

repeatedly elevated in EVs from extremely different cell types [6–9]. Phosphatidylserine, normally held on the inner membrane by flippase activity, becomes externalized during EV generation and is recognized as a hallmark of many EV surfaces [10–12]. In contrast, glycerolipids such as triacylglycerols are stored in intracellular lipid droplets [13] and are therefore depleted in EVs compared to the whole cell lipidomic pool [14,15]. These patterns suggest that EV formation follows a selective membrane budding process that enriches some lipid classes while depleting/excluding others. Examples of quantitative analysis supporting or refuting this hypothesis are lacking in the scientific literature.

It is generally accepted that EVs resemble their parent cell to some degree, but the resemblance has not been rigorously validated against a panel of unrelated cell lipidomes to determine whether these vesicles are truly distinguishable from non-origin cells. Also, the relationship between the EV lipidome and the systemic plasma lipidome remains poorly defined. Because plasma contains lipids contributed by many circulating cells and organs, it provides a useful reference for assessing how similar the EV lipidome is to the broader systemic lipid environment. Lastly, most cross-cell studies of EV lipidomics have been limited to a small number of cell types and lipid classes. Because of this, it remains unclear how strongly EV lipid composition varies across different organs and tissues.

We addressed these questions here using permutational multivariate analysis of variance and several other comparisons including broad lipidomic analysis. Our aim is to establish how closely EV lipidomes resemble their parent cells, how clearly they separate from unrelated cells and plasma, and how their composition is organized across cell lines of different tissue origin.

2. Materials and Methods

2.1. Workbench Datasets

For this study we used five lipidomic datasets detailed in Table S1. The HEK293T whole cell lipidome was generated using untargeted LC-MS/MS in both positive and negative ion modes. This dataset contained 8823 lipids across 18 samples representing six treatment groups. This dataset has been deposited in the Metabolomics Workbench under study identifier ST005020 [16]. For our analysis, we only used the three untreated control samples as the HEK293T whole cell reference. Next, the HEK293T EV lipidome was obtained from Metabolomics Workbench study ST004002 [17]. This lipidomics study provides a lipid atlas of EVs isolated by size exclusion chromatography from nine mammalian cell lines including HEK293T, B16, E0771, MB49-luc2, MC38, Melan-A, SK-Mel28, Yumm1.7, and Yummer. EV isolation for this dataset was performed by the original investigators and we relied on their reported adherence to community reporting standards for EV studies [18]. For this atlas, the positive and negative ion datasets contained 332 and 279 lipid features, respectively. For combining the two ion modes we excluded blank and pooled quality-control injections. This added up to 611 ion-mode-specific lipid features across 36 biological EV samples representing nine cell lines with four replicates per cell line.

Additionally, we used whole cell lipidomes from non-HEK293T cells obtained from Metabolomics Workbench. The $CD4^+$ T-cell lipidomic dataset was obtained from ST001676 [19] which was an untargeted LC-MS study of human $CD4^+$ T cells. From this study we used the Th0 samples which represent activated but undifferentiated T cells for a neutral reference. This data included 15 Th0-labeled samples from five donors. Each of the five donors contributed three Th0 profiles. These 15 profiles were averaged within each donor to give five independent Th0 profiles used in downstream analysis. The HuH-7 lipidome was from ST000685 [20]. For this data we used the six control samples which included three empty vector controls and three non-targeting shRNA controls. Lastly, the human plasma lipidome was from study ST003897 [21]. This was a postprandial lipidomics study of 147 healthy individuals. Only fasting baseline plasma samples were used, allowing plasma to serve as a systemic lipidome reference.

HEK293T is an established human embryonic kidney-derived cell line. HEK293T was selected because it was the only cell line in our analysis with available lipidomic data from both whole cells and EVs. As HEK293T is an immortalized cell line, these findings should be tested in additional cell types. HEK293T cells used to generate the whole-cell lipidomics data were obtained from ATCC (CRL-3216) and cultured at the Miami Integrative Metabolomics Research Center. The EV datasets from HEK293T, B16, E0771, MB49-luc2, MC38, Melan-A, SK-Mel28, Yumm1.7 and Yummer were obtained from Metabolomics Workbench study ST004002. The culture conditions of these cell lines were reported by the original investigators. The HuH-7 cell line data was obtained from Metabolomics Workbench study ST000685. Culture conditions again were reported in the associated study record. No previously unpublished or de novo cell lines were generated in the present study.

2.2. Data Processing

All datasets were processed in R (version 4.6.0) using a reproducible pipeline. For Workbench mwTab files, the data was extracted and converted into numeric matrices with the lipid species names as row identifiers. All equivalent lipid class labels were harmonized across studies. In the ST000685 dataset, lipid names included adduct and retention time information. These suffixes were removed by deleting text after the semicolon, leaving only lipid names. Lipids that were detected in both ion modes were retained with row identifiers during matrix construction. Lipid annotations were standardized to sum composition, and duplicate annotations were collapsed before overlap and correlation analysis.

For the HuH-7 dataset, positive and negative ion mode files were processed separately. Each file was first normalized to the percentage of total lipid signal in each sample. The two ion modes were then combined after adding mode specific prefixes to the row names, preventing duplicate names for lipid classes detected in both modes.

In all datasets lipid abundance was expressed as a percentage of total lipid signal per sample. For class level analyses, species level percentages were summed within each lipid class for every sample. Then, class means and standard deviations were calculated across samples within each set of data (Table S2).

2.3. Multivariate Statistical Analysis

Class level percentage matrices were generated for each data set, merged by lipid class, and then filled with zeros for classes absent from individual datasets. The matrices were Hellinger-transformed using the *decostand* function in the R package *vegan* (v2.6) before distance-based analysis and ordination. This approach is necessary for compositional abundance data and reduces the influences of shared absences [22].

Principal component analysis was performed using *prcomp* with centering and without scaling. Group level differences in lipid composition were tested by PERMANOVA using *adonis2* with Bray-Curtis dissimilarity and 999 permutations. Bray-Curtis dissimilarities were calculated using *vegdist* on class level mean abundance matrices as well when comparing the nine EV cell lines. Lastly the Pairwise PERMANOVA was performed across all group pairs with Benjamini-Hochberg adjustment (Tables S3–S7). The observed differences may reflect both true biological variation and technical differences as each biological group in the cross-study comparison came from a different dataset with different laboratory workflows. As source study and biological group are completely confounded, a separate batch analysis would not be informative.

2.4. Species Level Analysis

Lipid species overlap between HEK293T whole cell lipidomics and HEK293T EV lipidomics was determined by matching lipid species names after standardization. Species detected in both datasets were counted as shared. To determine if EVs preserved the same lipid species patterns as their parent cell we compared the rank order of shared lipids within each lipid class. For each dataset, lipid species were ranked by their average abundance across samples, and Spearman correlation was used to measure how similar those rankings were between the two datasets. Lipid classes with fewer than three shared species were excluded. Standardized species with mean abundances equal to zero across samples were excluded before overlap count. Spearman correlation p-values were adjusted using Benjamini-Hochberg method (Tables S8–S10).

2.5. Figures

Exploratory figures and tables were generated in R using *ggplot2* v3.5 and *pheatmap* v1.0.12. Final figures were then recreated and refined in GraphPad Prism 11 using the R-derived tables to improve presentation quality. For the heatmap, lipid classes were z-score scaled across cell lines, and clustering was performed using Ward.D2 clustering of Euclidean distances. EV enrichment ratios were expressed as log2(EV class percentage/whole cell class percentage). Lipid classes were classified as enriched or depleted using a 1.5 fold change threshold, corresponding to log2 ratios greater than 0.58 or less than -0.58 respectively. Classes below 0.1% mean in either fraction were excluded from all ratio calculations.

3. Results

3.1. HEK293T EVs Retain Core Features of Their Parental Cell Lipidome

When comparing the EV dataset to the HEK293T whole cell dataset we found many similarities between lipid classes, signatures, and abundance patterns. Of the 28 lipid classes quantified across both datasets, phosphatidylcholine (PC) was the single most abundant class in both, from 74.7% of the total lipid signature in

cells to 54.3% in EVs (Figure 1). Despite the reduction of PC seen in EVs, the major glycerophospholipid framework of the whole cell was preserved in EVs. Membrane lipid classes including phosphatidylethanolamine (PE), phosphatidylserine (PS), phosphatidylinositol (PI), and lysophosphatidylcholine (LPC), were observed in both parental cell and EV lipidomes, indicating that EVs retain the broad lipid architecture of their cells of origin while undergoing specific remodeling.

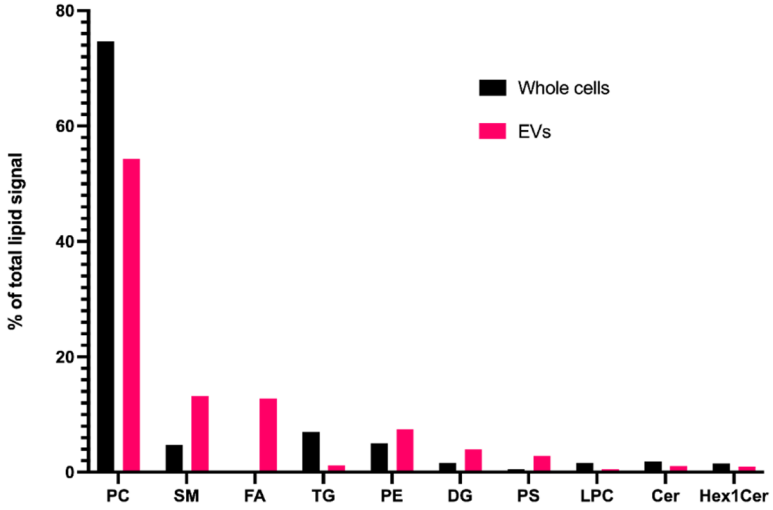


Figure 1. Lipid class composition of HEK293T whole cells versus HEK293T extracellular vesicles (EVs). EVs share the major lipid classes of their parent cells, but proportions shift. Bars show the percentage of lipid signal contributed by each lipid class in EVs (pink) and whole cells (black). Phosphatidylcholine (PC) dominated both fractions. Sphingomyelin (SM) and diacylglycerol (DG) are enriched in EVs compared to whole cells. Triglycerides (TG) are relatively depleted in EVs when compared to whole cells.

Although the EVs preserved their parent cell's general lipid architecture, they also showed a clear class specific sorting pattern (Figure 2). Sphingomyelin and phosphatidylserine were enriched in EVs, increasing 2.8-fold and 5.0-fold respectively when compared to the whole cell. On the other hand, triglycerides, LPC and PI were markedly reduced when comparing EVs to their parent cell, indicating that not all cellular lipid classes are incorporated into EVs equally.

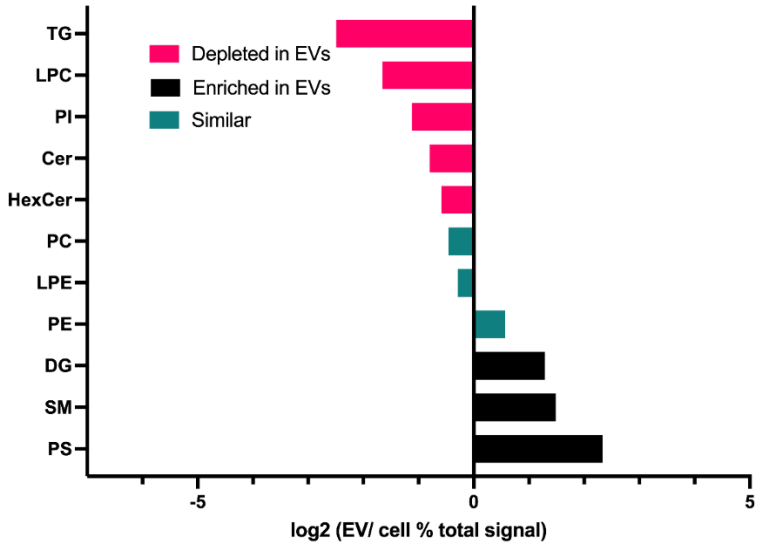


Figure 2. Selective lipid sorting during EV biogenesis. Horizontal bar chart displaying the log2 ratio of EV to parent cell percentage of total lipid signal for each lipid class. Classes with positive values (black) are enriched in EVs relative to cells, including PS, SM, and DG. Classes with negative values (pink) are depleted in EVs, most notably PI, TG, Cer and LPC. Classes with similar values (teal) between the two include PE, LPE, and PC. These findings indicate that EV biogenesis involves active and selective lipid sorting rather than passive membrane budding.

Individual species of lipids told a complementary story. Of the 334 lipid species detected in EVs, 241 or 72.2% were also found in the parental HEK293T cell. 93 lipid species were unique to vesicles and a further 407 were seen only in whole cells (Figure 3). Where species overlapped, their abundances tended to keep the same rank order in cells and EVs meaning that the internal lipid hierarchy of each was largely preserved across the two datasets. This relationship was strongest for PI (*rho* = 0.73), PE (*rho* = 0.74), and PC (*rho* = 0.48), the only three classes to survive Benjamini-Hochberg correction. It was weakest for TG (*rho* = 0.25) where the relatively low TG species seen in EVs suggest selective retention of only a subset of cellular triglyceride species.

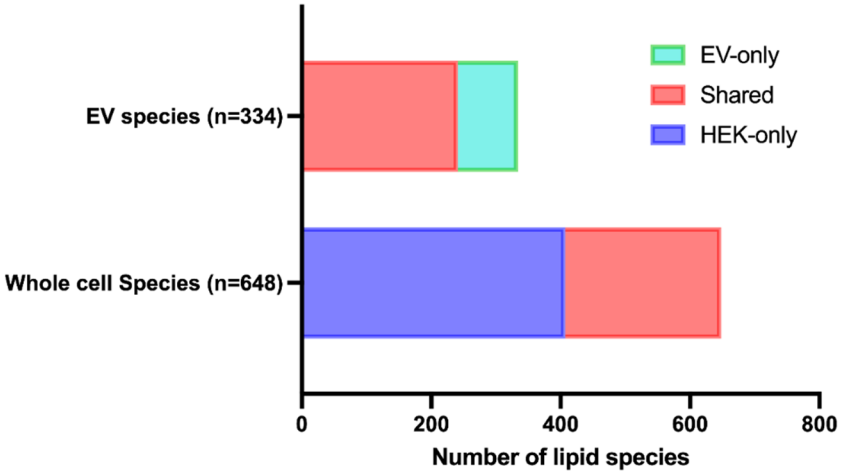


Figure 3. Most extracellular vesicles (EV) lipids are found in whole cells. Overlap between EV and parent cell lipidomes. Stacked horizontal bar chart comparing the number of lipid species detected in HEK293T-derived EVs (n = 334) and HEK293T whole cells (n = 648). 241 species were shared. Most of the EV lipid species are shared with the parent cell (red), with a small subset detected exclusively in EVs (teal). The cell lipidome is substantially broader, with a large proportion of species not detected in EVs (blue), demonstrating that EVs carry a fingerprint of the cellular lipidome rather than a complete representation.

3.2. HEK293T EVs Are Compositionally Distinct from Unrelated Cellular Lipidomes

PCA of Hellinger transformed lipid class composition showed clear separation among the four cell groups: HEK293T EVs, HEK293T whole cells, $CD4^+$ T cells, and HuH-7 hepatocytes. Each group formed a distinct non-overlapping cluster along PC1 and PC2 which explained 59.3% and 30.5% of the variance respectively (Figure 4A). PERMANOVA further confirmed this strong separation, with group identity explaining 96.5% of variance in lipid class composition ($F = 127.2$, $R^2 = 0.965$, $p = 0.001$).

All pairwise comparisons were significant after Benjamini-Hochberg correction, but the effect sizes provided additional insight into the relationships of the groups. The smallest separation was seen between HEK293T whole cell and its EV counterpart ($R^2 = 0.848$, $p = 0.022$). The largest separations were seen when comparing the HEK293T EVs to the $CD4^+$ T cells ($R^2 = 0.970$, p adjusted = 0.022) and the HuH-7 hepatocytes ($R^2 = 0.914$, p adjusted = 0.021). These comparisons show that the lipidome of HEK293T EVs is most similar to that of their parent cells, while remaining compositionally distinct from unrelated cellular lipidomes. Lastly, when comparing the $CD4^+$ T cells to the HuH-7 hepatocytes, the lipidomes were highly distinct from each other ($R^2 = 0.967$, p adjusted = 0.021), reflecting the differences between the liver and immune-derived cellular lipidomes.

Class composition comparison helps explain the basis for these separations. The HuH-7 hepatocyte lipidome is dominated mainly by free fatty acids (32.3%) and triglycerides (23.1%), reflecting the role of hepatocytes in fatty acid uptake, storage and neutral lipid export [23]. The T-cell lipidome had a high sphingomyelin fraction (31.5%) in line with the sphingomyelin rich membranes reported for lymphocytes [24].

3.3. HEK293T EVs and Whole Cells Both Differ from Healthy Plasma

Along with the previous comparisons we compared the relationship of EVs and their parent cells to healthy human plasma to see if these lipidomes could be distinctly separated from the human plasma lipidome. In a PCA comparing these three classes, plasma separated clearly from both cell-derived groups along PC1, PC1 explaining 39.9% of the variance in lipid class composition (Figure 4B). PERMANOVA again confirmed a significant overall

difference among groups (F = 52.6, R^2 = 0.411, p = 0.001). This comparison included HEK293T whole cells n = 3, HEK293T EVs n = 4, and fasting plasma n = 147.

This separation reflects the very distinct lipid compositions of plasma. Compared with cellular samples, plasma contained a higher triglyceride fraction, and broad representation of lipid classes such as DG, Cer, HexCer, and more. This pattern reflects the idea that plasma lipid content is shaped by many different circulating lipoproteins contributed by many different tissues.

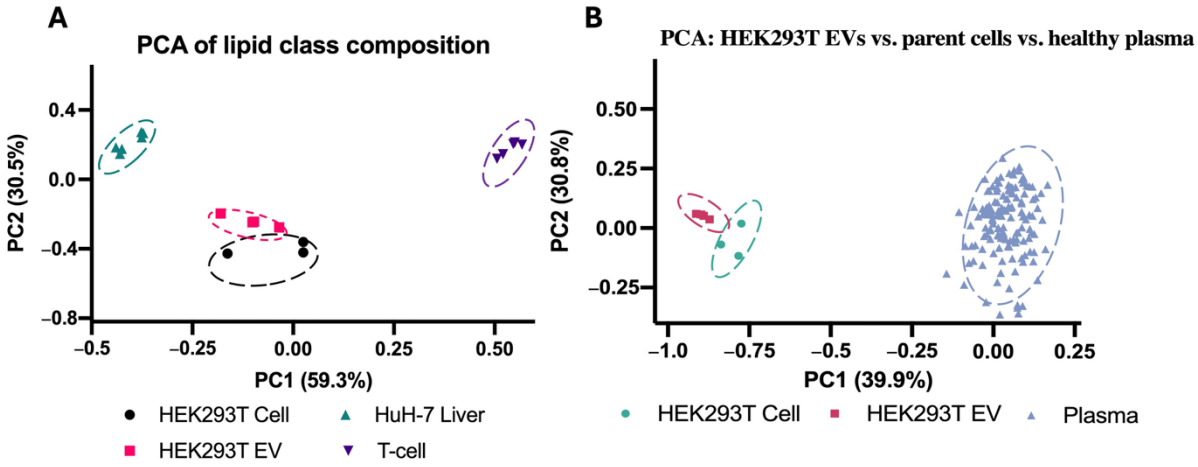


Figure 4. (**A**) Extracellular vesicles are compositionally distinct from cells they didn't come from (non-parental cells). Principal component analysis (PCA) of lipid class composition across cell types and EVs. Each point represents a biological replicate while dashed ellipses indicate grouping by sample. HEK293T cells (black) and HEK293T derived EVs (pink) resolve into distinct clusters separated primarily along PC1 (59.3%), showing distinct lipid class composition between the HEK293T EV and whole cell datasets. HuH-7 liver cells (teal) and T cells (purple) occupy separate regions of PC space, demonstrating that lipid class composition reflects both cell of origin and EV remodeling. (**B**) Both EVs and parent cells are clearly separated from the systemic plasma lipidome. PCA comparing HEK293T EVs, parent cells, and healthy human plasma. EVs (pink) and parent cells (green) cluster tightly together in the lower-left quadrant, separated from the healthy plasma lipidome (light blue triangles). The plasma samples show greater internal variance along PC2 (30.8%), likely reflecting biological heterogeneity across donors. The large PC1 separation indicates that EV and cellular lipidomes are fundamentally distinct from the circulating plasma lipid environment, underscoring the need for caution when using plasma as a reference in EV biomarker studies. Because each group came from a different source dataset, the observed separation may reflect both biological variation and technical differences between the studies. Group sizes for these comparisons included n = 3 for HEK293T whole cells, n = 4 for HEK293T EVs, n = 5 for T cells, n = 6 for HuH-7 cells, and n = 147 for plasma.

3.4. EV Lipidomes Vary by Their Cell and Tissue of Origin

Lastly, we compared lipid class composition across nine EV datasets using Bray-Curtis dissimilarity to see whether EV lipidomes differ by origin (Figures 5 and 6). Each of the nine EV cell lines included four biological replicates (n = 4). In our analysis we found the EV profiles separated based on their source cell type. This confirms that EV lipid composition is not uniform across all cell lines and tissues. The most intense signal outlier came from the E0771 breast cancer EVs. This line showed the highest dissimilarity from other EV datasets with a Bray-Curtis dissimilarity of 0.62 relative to HEK293T. The E0771 cell line was distinct due to its higher DG and FA levels and low PC content. FA was retained in this comparison as all nine EV cell lines were analyzed within the same ST004002 dataset. This differs from the EV versus whole cell HEK293T studies which combined data from separate studies.

On the other hand, HEK293T EVs were most similar to MC38 colon cancer EVs (Bray-Curtis dissimilarity = 0.043). The Yummer and Yumm1.7 melanoma EVs were also relatively close to the HEK293T EVs with a Bray-Curtis dissimilarity of 0.111 and 0.110 respectively. Although tissue of origin broadly organized EV lipidome variation, cell-line-specific differences remained. The five Melanocytic EV datasets did not form one cluster, suggesting that individual cell line differences can strongly influence EV lipid composition even within the same melanocytic lineage. PC remained the dominant lipid class in eight out of the nine EV cell-lines with E0771 being dominated by FA instead.

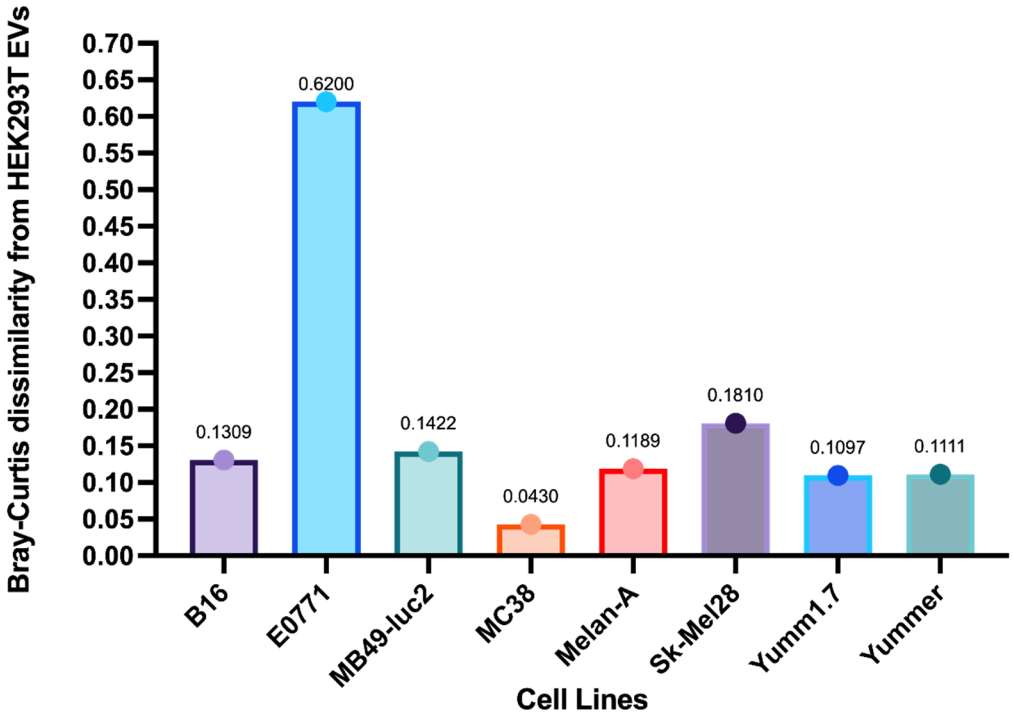


Figure 5. EV lipidome composition varies across cell lines. Bray-Curtis dissimilarity of EV lipidomes from diverse cell lines relative to HEK293T derived EVs. Melanocytic derived EVs (Yumm1.7, Yummer, Melan-A, B16, Sk-Mel28; multi-colored) and bladder cancer EVs (MB49-luc2; green) cluster at low-to-intermediate dissimilarity values (0.110 to 0.181), while colon cancer EVs (MC38; orange) are the most similar to HEK293T EVs (0.043). Breast cancer EVs (E0771; blue) are strikingly dissimilar (0.620), suggesting that tissue of origin is a dominant driver of EV lipidome identity.

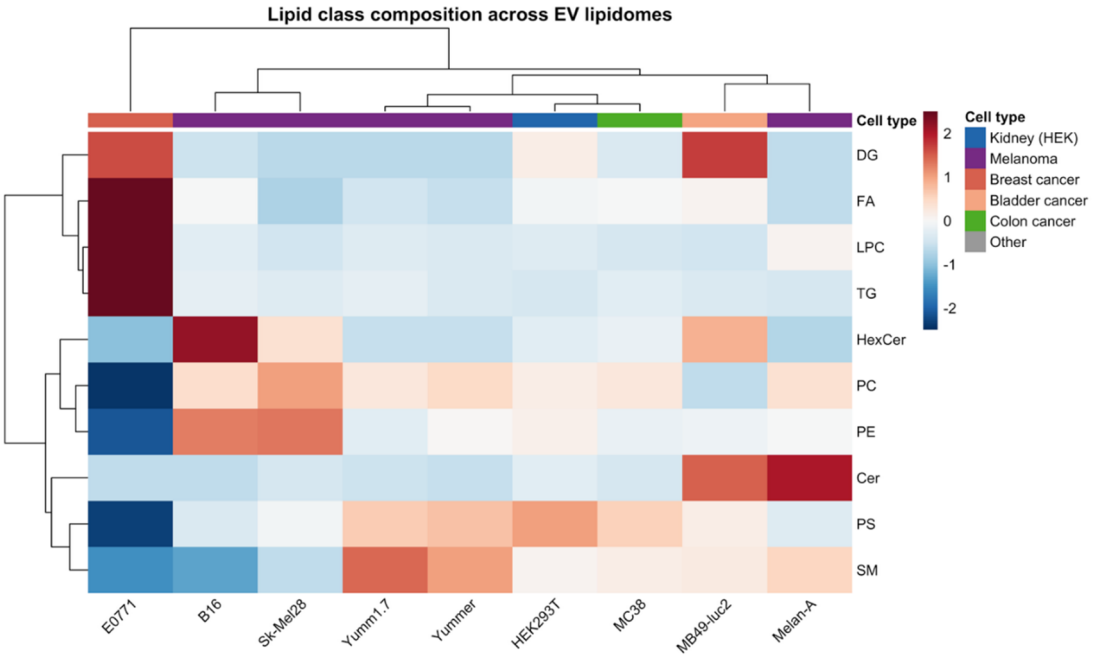


Figure 6. Tissue of origin organizes EV lipidome diversity across cell lines. Hierarchical clustering heatmap of lipid class composition across EV lipidomes from nine cell lines. Color intensity reflects z-scored lipid class abundance (red = enriched, blue = depleted). Cell lines are annotated by tissue of origin (top color bar). The breast cancer line clusters separately from all others, driven by pronounced enrichment of FA, LPC, and TG and depletion of PC and PE. Melanocytic lines (Yumm1.7, Yummer, Sk-Mel28, B16, Melan-A) showed related heatmap profiles with intermediate composition. HEK293T and MC38 colon cancer EVs clustered closely together, whereas MB49-luc2 bladder cancer EVs clustered with Melan-A EVs.

4. Discussion

Together, these findings make a case that EV lipidomes are not just random reflections of their parent cells, but selectively remodeled membrane profiles. Three major findings stand out.

First, HEK293T EVs resemble their parent cell more than the unrelated cell types we examined, yet they are not miniature copies of their parental cell. The relative depletion of TG, LPC and PI and the abundant enrichment of SM and PS suggest a coherent lipid sorting signature. This pattern is consistent with selective membrane remodeling during EV biogenesis. The SM enrichment fits the idea that sphingolipid-rich membrane domains contribute to intraluminal vesicle formation within multivesicular bodies [7,25]. The PS enrichment is consistent with changes in membrane asymmetry during EV budding. Reduced flippase activity and increased scramblase activity may promote PS redistribution into the budding EV membrane [10,11]. Lastly, the marked loss of TG is biologically consistent. TGs are primarily stored in lipid droplets and not typically incorporated into EV membranes [13,14].

Second, the EV and parent cell lipidomes differ from healthy plasma, and this highlights the need for plasma EV work. In circulation EVs are surrounded by lipoproteins which make up a large fraction of the plasma lipid pool [26]. Because vesicle lipidomes are compositionally distinct from plasma lipidomes, any lipoprotein contamination during EV isolation would pull the measured profile towards the plasma signature and away from the true vesicle composition. This barrier underscores the need for rigorous separation of EVs from plasma lipoproteins for clean EV lipidome results.

Lastly, EV lipidome diversity when comparing the nine EV cell lines was mainly organized by tissue of origin. An independent panel of cancerous and non-cancerous lines reached a similar conclusion, with EV lipid profiles clustering apart from their cell of origin while retaining features dictated by tissue of origin [27]. However, within type variation remained. The E0771 breast cancer EVs provided the clearest example of distinct lipid profile, which may be due to the high lipid droplet content and lipid metabolism described in many mammary cancer cells [28,29]. On the other hand, the colon cancer and HEK293T cell lines clustered closely together despite their unrelated origins in embryonic kidney and colon. This may suggest that some EV lipidomic features may be conserved across cell lines, even in different tissues.

This study had the following limitations. First, pooling datasets on different instruments, with different extraction protocols and ion modes, introduces batch effects that harmonization cannot remove entirely. Working from the level of lipid classes blunts this problem, since proportions travel across platforms more reliably than abundances of lipid species, but it cannot eliminate it. Next, the T-cell dataset was acquired in positive ion mode alone. This means that classes that ionize best in the negative ion mode are likely underrepresented within this dataset. The HuH-7 group had only six control samples which limits the statistical power available for the comparisons between the HuH-7 group. Free fatty acids were detected at only 0.003% of whole cell lipid signal versus 12.8% in EVs. This gap is more consistent with extraction and ionization differences between studies than with biology. Because of this FA ratios were excluded from enrichment and ratio analysis in our cross-study analysis. Another limitation is that EV isolation was performed independently across studies and adherence to current standards [18] varies by dataset. Because biological group and dataset source were linked in the cross-study comparisons, separations cannot be fully attributed to biology alone. On the other hand, the nine EV cell line comparison is less affected as all groups came from the same study (ST004002). Finally, the small whole cell HEK293T ($n = 3$) and HuH-7 ($n = 6$) groups may reduce the stability of the estimated PERMANOVA effect sizes.

Two further directions follow naturally. The first is to test whether the parent cell resemblance of EVs holds for non-immortalized cell lines, and whether disease-driven shifts in the cellular lipidome are passed on proportionally to vesicle lipidomes. The second direction is methodological. Answering these questions at a larger scale will require greater standardization of EV lipidomic workflows across laboratories. Public repositories such as Metabolomics Workbench are well positioned to support this effort by improving data sharing and cross-study comparison.

5. Conclusions

In conclusion, these results show that HEK293T EVs keep a clear connection to their parent cell, but they are not simple copies. The extracellular vesicle lipidome shared much of the same core structures as the whole cell lipidome with 72.2% of the detected species overlapping between the two. At the same time, EVs showed selective remodeling including enrichment of SM and PS and loss of TG, suggesting that vesicle biogenesis reshapes the inherited lipid framework. HEK293T EVs also remained more similar to their cell of origin than to unrelated cell lipidomes or healthy plasma. Within HEK293T, this is evidence that EV lipidomes carry a meaningful fingerprint from their parent cell. This comparison was limited to the HEK293T cell line, so further validation in multiple matched cell and EV systems will be needed to determine generalizability. Across the nine EV comparison datasets

we found that lipid composition also varied by cellular source and line. These findings support EV lipidomics as a useful approach to study vesicle biology, cell identity, and membrane remodeling. A graphical summary is provided in Figure 7.

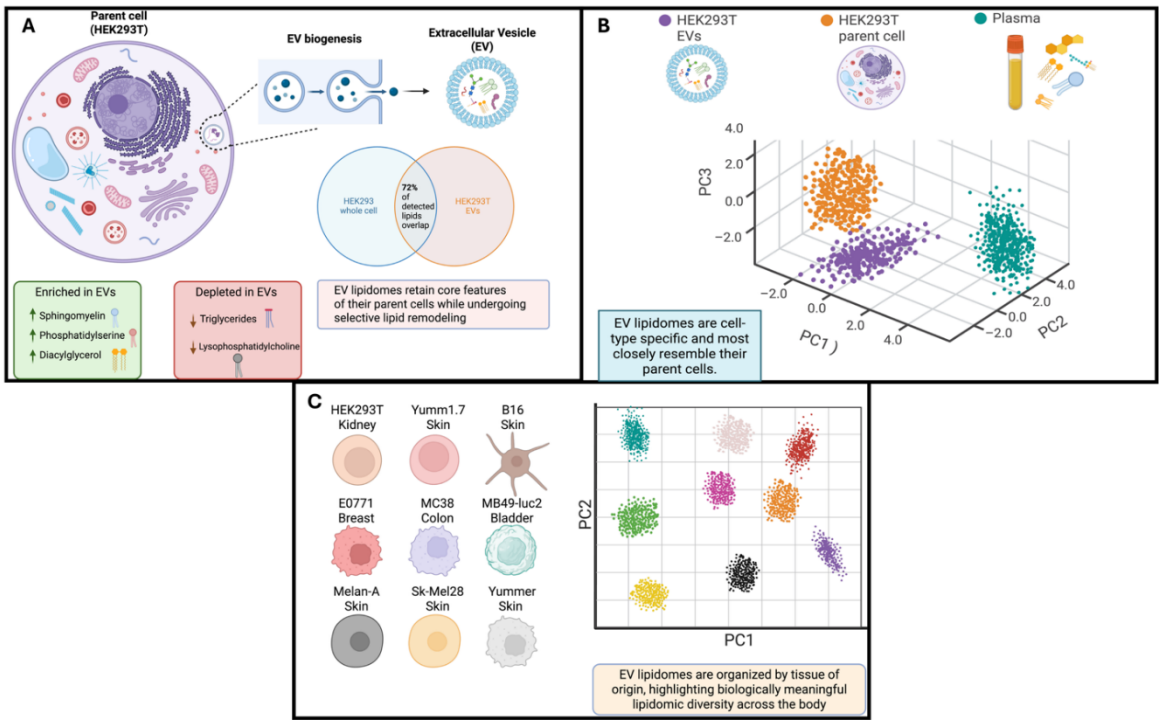


Figure 7. (**A**) Overview of extracellular vesicle biogenesis from HEK293T parent cells and the resulting EV lipid composition. EVs share a large portion of their lipidome with the parent cell, with 72.2% of detected lipids overlapping between HEK293T whole cells and HEK293T EVs. Despite this overlap, EVs show selective lipid remodeling. EVs are enriched in sphingomyelin, phosphatidylserine, and diacylglycerol, and depleted of triglycerides, phosphatidylinositol, and lysophosphatidylcholine. (**B**) Conceptual principal component analysis comparing HEK293T EVs, HEK293T parent cells, and plasma demonstrates that EV lipidomes are compositionally distinct from plasma and cluster most closely with their parent-cell lipid profile. (**C**) Conceptual cross-cell-type comparison of EV lipidomes from kidney, breast, colon, bladder, and skin-derived cells shows most reliable separation by tissue or cell type.

Supplementary Materials

The additional data and information can be downloaded at: https://media.sciltp.com/articles/others/26101 21350012788/TI-26070209-SM.zip.

Author Contributions

S.K.B.: Article conception and writing (review and editing). K.P.: Data curation, analysis, investigation, writing (original draft). K.K.: Methodology, validation and writing (review and editing). All authors have read and agreed to the submitted version of the manuscript.

Funding

This work was supported in part by the Doris L. Hastings Foundation, Leonard and Norma Klorfine Foundation, Sydney and Elizabeth Ross Family Foundation, and an unrestricted grant from Research to Prevent Blindness to the University of Miami. Kyle Peres was supported by a Singerman and Schwartz Fellowship.

Institutional Review Board Statement

This study used publicly available, de-identified datasets and did not involve recruitment of human participants or private information. No additional review board approval was required for this analysis.

Informed Consent Statement

Not applicable to the analysis. Informed consent requirements for the original studies were addressed by the original investigators.

Data Availability Statement

The public lipidomic datasets are available from the Metabolomics Workbench repository under study identifiers ST004002, ST000685, ST001676, and ST003897. The HEK293T whole-cell lipidomics data generated in this study have been deposited in the Metabolomics Workbench under study identifier ST005020 (DOI: 10.21228/M8Z86M). This can be found at the following URL: https://metabolomicsworkbench.org/data/DRCCMetadata.php?Mode=Study&StudyID=ST005020. The R analysis pipeline used for all datasets is archived on Zenodo (DOI: https://doi.org/10.5281/zenodo.21419380).

Conflicts of Interest

The authors declare no conflict of interest.

Use of AI and AI-Assisted Technologies

No AI tools were utilized for this paper.

Reproduction Statement

This article is republished here with permission from all authors and the former editorial team of *Biomolecular Mechanisms and Innovations*, which has discontinued publication. No editorial changes have been made from the original publication. Original publication: Peres, K.; Kishor, K.; Bhattacharya, S.K. HEK293T Vesicle Lipidomes Retain Core Features of Their Parent Cells. *Biomolecular Mechanisms and Innovations* **2026**, *1*(1), 4.

References

1. Kalluri, R.; LeBleu, V.S. The biology, function, and biomedical applications of exosomes. *Science* **2020**, *367*, eaau6977. https://doi.org/10.1126/science.aau6977.
2. van Niel, G.; D'Angelo, G.; Raposo, G. Shedding light on the cell biology of extracellular vesicles. *Nat. Rev. Mol. Cell Biol.* **2018**, *19*, 213–228. https://doi.org/10.1038/nrm.2017.125.
3. Dixson, A.C.; Dawson, T.R.; Di Vizio, D.; et al. Context-specific regulation of extracellular vesicle biogenesis and cargo selection. *Nat. Rev. Mol. Cell Biol.* **2023**, *24*, 454–476. https://doi.org/10.1038/s41580-023-00576-0.
4. Liu, Y.J.; Wang, C. A review of the regulatory mechanisms of extracellular vesicles-mediated intercellular communication. *Cell Commun. Signal.* **2023**, *21*, 77. https://doi.org/10.1186/s12964-023-01103-6.
5. Fonseka, P.; Mathivanan, S. Extracellular Vesicles Biogenesis, Cargo Sorting and Implications in Disease Conditions. *Cells* **2023**, *12*, 280. https://doi.org/10.3390/cells12020280.
6. Record, M.; Carayon, K.; Poirot, M.; et al. Exosomes as new vesicular lipid transporters involved in cell-cell communication and various pathophysiologies. *Biochim. Biophys. Acta Mol. Cell Biol. Lipids* **2014**, *1841*, 108–120. https://doi.org/10.1016/j.bbalip.2013.10.004.
7. Skotland, T.; Hessvik, N.P.; Sandvig, K.; et al. Exosomal lipid composition and the role of ether lipids and phosphoinositides in exosome biology. *J. Lipid Res.* **2019**, *60*, 9–18. https://doi.org/10.1194/jlr.r084343.
8. Skotland, T.; Llorente, A.; Sandvig, K. Lipids in extracellular vesicles: What can be learned about membrane structure and function? *Cold Spring Harb. Perspect. Biol.* **2023**, *15*, a041415. https://doi.org/10.1101/cshperspect.a041415.
9. Rome, S.; Tacconi, S. High-fat diets: You are what you eat…your extracellular vesicles too! *J. Extracell. Vesicles* **2024**, *13*, e12382. https://doi.org/10.1002/jev2.12382.
10. Fujii, T.; Sakata, A.; Nishimura, S.; et al. TMEM16F is required for phosphatidylserine exposure and microparticle release in activated mouse platelets. *Proc. Natl. Acad. Sci. USA* **2015**, *112*, 12800–12805. https://doi.org/10.1073/pnas.1516594112.
11. Bevers, E.M.; Williamson, P.L. Getting to the outer leaflet: Physiology of phosphatidylserine exposure at the plasma membrane. *Physiol. Rev.* **2016**, *96*, 605–645. https://doi.org/10.1152/physrev.00020.2015.
12. Perez, G.; Bernard, M.; Vocelle, D.; et al. Phosphatidylserine-exposing annexin A1-positive extracellular vesicles: Potential cancer biomarkers. *Vaccines* **2023**, *11*, 639. https://doi.org/10.3390/vaccines11030639.
13. Walther, T.C.; Farese, R.V., Jr. Lipid droplets and cellular lipid metabolism. *Annu. Rev. Biochem.* **2012**, *81*, 687–714. https://doi.org/10.1146/annurev-biochem-061009-102430.

14. Ghadami, S.; Dellinger, K. The lipid composition of extracellular vesicles: Applications in diagnostics and therapeutic delivery. *Front. Mol. Biosci.* **2023**, *10*, 1198044. https://doi.org/10.3389/fmolb.2023.1198044.
15. Blandin, A.; Dugail, I.; Hilairet, G.; et al. Lipidomic analysis of adipose-derived extracellular vesicles reveals specific EV lipid sorting informative of the obesity metabolic state. *Cell Rep.* **2023**, *42*, 112169. https://doi.org/10.1016/j.celrep.2023.112169.
16. Bhattacharya, S. Untargeted Lipidomic Analysis of HEK293T Cells after Fatty Acid Synthesis Inhibition [Dataset]. NIH Common Fund's National Metabolomics Data Repository (NMDR), Metabolomics Workbench; 2026 [Study ID: ST005020. https://doi.org/10.21228/M8Z86M]. Available online: https://metabolomicsworkbench.org/data/DRCCMetadata.php?Mode=Study&StudyID=ST005020 (accessed on 9 September 2026).
17. Drotleff, B. A Deep, Quantitative Lipid Atlas of Extracellular Vesicles across Multiple Cell Lines. [Dataset]. NIH Common Fund's National Metabolomics Data Repository (NMDR), Metabolomics Workbench; 2025 [Study ID: ST004002; Project ID: PR2507; Project DOI: 10.21228/M8KN8R]. Available online: https://www.metabolomicsworkbench.org/data/DRCCMetadata.php?Mode=Study&StudyID=ST004002&StudyType=MS&ResultType=1 (accessed on 10 August 2026).
18. Welsh, J.A.; Goberdhan, D.C.I.; O'Driscoll, L.; et al. Minimal Information for Studies of Extracellular Vesicles (MISEV2023): From Basic to Advanced Approaches. *J. Extracell. Vesicles* **2024**, *13*, e12404. https://doi.org/10.1002/jev2.12404.
19. Sen, P. Lipidomic Analysis of $CD4^+$ T-cell subsets (Th1, Th2, Th17 and iTreg cells) (part I) [Dataset]. NIH Common Fund's National Metabolomics Data Repository (NMDR), Metabolomics Workbench; 2021 [Study ID: ST001676; Project ID: PR078. https://doi.org/10.21228/M8C111]. Available online: https://www.metabolomicsworkbench.org/data/DRCCMetadata.php?Mode=Study&StudyID=ST001676 (accessed on 10 August 2026).
20. Kachman, M. Lipidomics Analysis for Human Liver Cell Lines [Dataset]. NIH Common Fund's National Metabolomics Data Repository (NMDR), Metabolomics Workbench; 2018 [Study ID: ST000685; Project ID: PR484. https://doi.org/10.21228/M8H03P]. Available online: https://www.metabolomicsworkbench.org/data/DRCCMetadata.php?Mode=Study&StudyID=ST000685 (accessed on 10 August 2026).
21. Wang, J. Postprandial Plasma Lipidomic Changes in 147 Individuals Following Ingestion of a Standard Mixed Meal. Available online: https://metabolomicsworkbench.org/data/DRCCMetadata.php?Mode=Study&StudyID=ST003897 (accessed on 10 August 2026).
22. Legendre, P.; Gallagher, E.D. Ecologically meaningful transformations for ordination of species data. *Oecologia* **2001**, *129*, 271–280. https://doi.org/10.1007/s004420100716.
23. Alves-Bezerra, M.; Cohen, D.E. Triglyceride metabolism in the liver. *Compr. Physiol.* **2017**, *8*, 1–22. https://doi.org/10.1002/cphy.c170012.
24. Zech, T.; Ejsing, C.S.; Gaus, K.; et al. Accumulation of raft lipids in T-cell plasma membrane domains engaged in TCR signalling. *EMBO J.* **2009**, *28*, 466–476. https://doi.org/10.1038/emboj.2009.6.
25. Trajkovic, K.; Hsu, C.; Chiantia, S.; et al. Ceramide triggers budding of exosome vesicles into multivesicular endosomes. *Science* **2008**, *319*, 1244–1247. https://doi.org/10.1126/science.1153124.
26. Sun, Y.; Saito, K.; Saito, Y. Lipid profile characterization and lipoprotein comparison of extracellular vesicles from human plasma and serum. *Metabolites* **2019**, *9*, 259. https://doi.org/10.3390/metabo9110259.
27. Douanne, N.; Benslimane, Y.; López, R.R.; et al. Lipidome analysis of cancer cells and their extracellular vesicles reveals cancer-type-specific lipid signatures and enables the design of EV-mimetic liposomes. *J. Extracell. Vesicles* **2026**, *15*, e70265. https://doi.org/10.1002/jev2.70265.
28. Menendez, J.A.; Lupu, R. Fatty acid synthase and the lipogenic phenotype in cancer pathogenesis. *Nat. Rev. Cancer* **2007**, *7*, 763–777. https://doi.org/10.1038/nrc2222.
29. Zhang, J.; Li, J.; Zheng, Y.; et al. Lipid metabolism and lipid signaling in extracellular vesicles ontogeny: From biogenesis to functional execution. *J. Nanobiotechnology* **2025**, *23*, 672. https://doi.org/10.1186/s12951-025-03769-1.